Application of Integral Transform on the Flow of Unsteady Fractionalized Oldroyd B Fluid

Fozia Shaikh[*], Khadija Shaikh[†], Afaque Ahmed Bhutto[‡], Kiran Zehra[§]

Abstract

This work studies the fractional flow of two infinite coaxial cylinders over Odroyd-B fluids. The fluid motion is produced by the combined effect of the inner cylinder's rotational motion and a time-dependent oscillating pressure gradient. The Caputo fractional operator, Laplace transforms, and the finite Hankel transform are used to produce the semi-analytical solution for flow velocity and shear stress. Furthermore, the results indicate that the flow depends on time, the fractional parameter, and the non-Newtonian parameter.

Keywords: Fractionalized Oldroyd-B Fluid; Integral Transforms; Caputo Operator; Oscillating Pressure Gradient.

Introduction

Fractional differential equations are considered to be the most effective means of describing physical and technical processes, which have been modelled using fractional calculus. It is important to remember that conventional mathematical models, particularly nonlinear models, of integer-order derivatives often fail to give appropriate results. Recent advances in a variety of disciplines, including biology, chemistry, control theory, signal and image processing, mechanics, electricity, and economics, have made fractional calculus extremely essential (Miller & Ross, 1993). Given these non-Newtonian fluids' non-linear behavior, researchers use various analytical and numerical techniques. Solving these kinds of flow issues has greatly advanced with fractional calculus. In the beginning, fractional calculus was used to solve time-dependent, viscous-diffusion fluid mechanics systems. Nevertheless, its application to non-linear flow problems has grown since it can provide memory data descriptions in addition to precise, semi-analytical results similar to those obtained with classical methods. The time-fractional Caputo derivative is used in research to study semi-analytical solutions for the time-dependent 1-dimensional flow of Generalized Maxwell fluids in channels (Rauf et

[*]Department of Basic Sciences and Related Studies, Mehran University of Engineering and Technology, Jamshoro 76090, Pakistan, fozia.shaikh@faculty.muet.edu.pk

[†]Corresponding Author: Department of Basic Sciences and Related Studies, Mehran University of Engineering and Technology, Jamshoro 76090, Pakistan, khadijadoqadir@gmail.com

[‡]Department of Basic Sciences and Related Studies, The University of Larkano, Larkana 77150, Pakistan, afaq_bhutto@uolrk.edu.pk

[§]Department of Basic Sciences and Related Studies, Mehran University of Engineering and Technology, Jamshoro 76090, Pakistan, kzehra2828@gmail.com

al., 2020). Detailed analysis on the time-dependence of viscous Maxwell fluid motion over wavering cylinders of the same axis with fixed outer cylinder using an integral transformation, was also performed by (Khalique et al., 2019).

Unsteady flow of Oldroyd-B fluid between two cylinders are diversely used in various engineering and scientific fields. For instance, in high-performance machinery, the lubrication of moving parts often involves non-Newtonian fluids. The rotating inner cylinder model helps in designing and improving lubricants for better performance and longevity of mechanical components. Also, such flow fluids in cylindrical geometries are applicable in polymer processing, oil and gas industry, chemical engineering and many other. Shaikh et al. (2022) uses fractional Caputo derivation to examine the behaviour of fractional Oldroyd B fluid between oscillating cylinders. In diverging from its applications in fluid dynamics, fractional calculus has found diverse utility across various disciplines. The Caputo fractional derivative is significant because it allows for the accurate modelling of systems with memory effects and non-local behaviours in mathematics and physics, while also accommodating non-zero initial conditions and being applicable to boundary value problems. Qureshi & Yusuf (2019) explores the fractionalization of the blood ethanol concentration model using various fractional operators, showcasing improved estimation compared to the integer-order model in certain cases. The authors investigate measles transmission dynamics using a novel epidemiological model incorporating both integer and fractional order operators. An investigation on the unsteady flow of flowing down the flow in the cylindrical tank has been taken using the analytical technique (Khaskheli et al., 2020). Tanveer et al. (2017) use the Fox H-function to analyze the magneto-hydrodynamic flow of a generalized Oldroyd-B fluid across an infinite oscillating plate with slip condition. A new fractional model is proposed by Qureshi et al. (2019) evaluates the effects of deforestation on wildlife. The study proves the existence and uniqueness of solutions, presents numerical simulations and comparative analysis, and highlights the model's insightful findings, surpassing previous studies. (Afaque et al., 2023) inquired the location of the inhibitor impacted the oscillation of pressure within a solid fuel combustion chamber.

Numerical approaches have been used to investigate the behaviour of mixing fluid flows in the chamber (Khokhar et al., 2024). It introduces a new system with stability analysis and computes the basic reproduction number using fractional conformable derivatives. Afaque et al. (2023) examined the flow of an incompressible fluid with variable viscosity and finite conductivity across an infinite plane when heat transfer and a

magnetic field were present. For the vorticity distribution proportional to an oscillating stream, general solutions were obtained. In this study, we chose to use Caputo fractional derivatives in deriving analytical results for velocity profile and shear stress distribution in the presence of oscillating pressure gradients of an oscillating cylinder of the same axis containing Oldroyd B liquid.

Theorizing the Problem

An Oldroyd B fluid between two infinite circular cylinders of radius R_1 and R_2 ($R_2 > R_1$) is considered (see Figure 1). In this theoretical study, the cylinders are in a resting position at $t = 0$. At time $t = 0^+$, when the transient pressure gradient is employed in the azimuthal direction, the inner cylinder is abruptly moved whereas the outer remains stationary. In this speculative position, consider the coordinates of the cylinder are (r, θ, z), taking the r-axes perpendicular and z-axis laterally with the axis of the cylinder simultaneously.

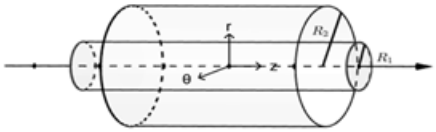

Figure 1: Problem geometry (Shaikh K, et al., 2022)

The conservation equation that governs the flow is described by,

$$\nabla \cdot \bar{V} = 0, \ \rho \frac{D\bar{V}}{Dt} = \nabla \cdot \bar{T}, \ \bar{T} = p\bar{I} + \bar{S} \tag{1}$$

Here velocity vector is symbolised by V, p defines pressure, and ρ, the constant density, whereas T signifies the Cauchy stress tensor. The constitutive equation apropos the flow of Oldroyd-B fluid gains attention in (Oldroyd & James, 1950):

$$\bar{S} + \lambda \left[\frac{\partial \bar{S}}{\partial t} + (\bar{V} \cdot \nabla)\bar{S} - \bar{L}\bar{S} - \bar{S}\bar{L}^T \right] = \mu \left\{ \bar{\gamma} + \lambda_r \left[\frac{\partial \bar{\gamma}}{\partial t} + (\bar{V} \cdot \nabla)\bar{\gamma} - \bar{L}\bar{\gamma} - \bar{\gamma}\bar{L}^T \right] \right\} \tag{2}$$

In this case, L is the velocity gradient (s^{-1}), S signifies the extra stress tensor (N/m^2), μ refers to dynamic viscosity (Ns/m^2), whereas λ implies the relaxation parameter, λ_r $(0 \leq \lambda_r < \lambda)$ symbolizes the retardation parameter, finally, the first Rivilan Erikson tensor is $\gamma = \nabla V + (\nabla V)^T$.

On presenting the fractional derivative, Equation 2 appears in the form:

$$\bar{S} + \lambda [D_t^{\alpha} \bar{S} + (\bar{V} \cdot \nabla)\bar{S} - \bar{L}\bar{S} - \bar{S}\bar{L}^T] = \mu \{ \bar{\gamma} + \lambda_r [D_t^{\alpha} \bar{\gamma} + (\bar{V} \cdot \nabla)\bar{\gamma} - \bar{L}\bar{\gamma} - \bar{\gamma}\bar{L}^T] \} \tag{3}$$

Where D_t^{α} is the Caputo fractional operator defined as:

$$D_t^{\alpha}h(t) = \begin{cases} \dfrac{1}{\Gamma(1-\alpha)}\displaystyle\int_0^t \frac{h'(x)}{(t-x)^{\alpha}}dx & 0 < \alpha < 1; \\ \dfrac{dh(t)}{dt} & \alpha = 1, \end{cases} \tag{4}$$

Since the flow is unsteady and moving in the circular cylinder, therefore the velocity field and extra stress S are functions of r and t,

$$\bar{\mathrm{V}} = \mathrm{v}(\mathrm{r},\mathrm{t})\mathrm{e}_{\theta}\,, \quad \bar{\mathrm{S}} = \mathrm{S}(\mathrm{r},\mathrm{t}) \tag{5}$$

Since both the geometry and fluid are primarily at rest, the value of time is zero, therefore,

$$\bar{V}(r,0) = 0 \; and \; \bar{S}(r,0) = 0 \tag{6}$$

Plugging Equation (3) in Equation (1), we obtain,

$$\rho(1+\lambda D_t^{\alpha})\tau(r,t) = \mu(1+\lambda_r D_t^{\alpha})\left(\frac{\partial}{\partial r} - \frac{1}{r}\right)v(r,t) \tag{7}$$

$$\rho(1+\lambda D_t^{\alpha})\frac{\partial v(r,t)}{\partial x} + \frac{1}{r}(1+\lambda D_t^{\alpha})\frac{\partial P}{\partial \theta} = \mu\left(1+\lambda_r D_t^{\delta}\right)\left(\frac{\partial^2}{\partial r^2} + \frac{1}{r}\frac{\partial}{\partial r} - \frac{1}{r^2}\right)v(r,t) \tag{8}$$

Where $S_{rr} = S_{zz} = S_{rz} = S_{\theta z} = S_{\theta\theta} = 0$, The nonzero shear stress is defined as $\tau(r, t) = S_{r\theta}(r, t)$, and the kinematic viscosity as $\upsilon = \mu/\rho$. In this study, we adopt time $t > 0$, $\partial P/\partial\theta = -\rho P_0 \cos(\omega t)$ where P_0 is a constant, so Equation (8) takes the form,

$$(1+\lambda D_t^{\alpha})\frac{\partial v(r,t)}{\partial x} - \frac{P_0}{r}(1+\lambda D_t^{\alpha})\cos(\omega t) = \upsilon\left(1+\lambda_r D_t^{\delta}\right)\left(\frac{\partial^2}{\partial r^2} + \frac{1}{r}\frac{\partial}{\partial r} - \frac{1}{r^2}\right)v(r,t) \tag{9}$$

The fractional parameters are identified as α and δ in such a way that $0 \le \alpha \le \delta \le 1$ is achieved. As a result, the boundary and initial conditions are as follows:

$$v(r,0) = \frac{\partial v(r,0)}{\partial t} = 0, \qquad r \in [R_1, R_2] \tag{10}$$

$$v(R_1,t) = \mathrm{fe}^{\mathrm{at}} \quad and \quad v(R_2,t) = 0, \quad r > 0 \tag{11}$$

Where f is a constant.

Computation of the Velocity Profile

Applying the Laplace transform illustrated by Debnath & Lokenath (2016) in Equation (9) and results in:

$$(s+\lambda s^{\alpha+1})\bar{v}(r,s) -$$

$$\frac{P_0}{r}\left(\frac{\omega}{s^2+\omega^2}+\lambda s^{\alpha}\left(\frac{s\sin\left(\frac{\pi}{2}\alpha\right)+\omega\cos\left(\frac{\pi}{2}\alpha\right)}{s^2+\omega^2}\right)\right)=$$
$$\upsilon\left(1+\lambda_r s^{\delta}\right)\left(\frac{\partial^2}{\partial r^2}+\frac{1}{r}\frac{\partial}{\partial r}-\frac{1}{r^2}\right)\bar{v}(r,s) \quad (12)$$

Since

$$(s+\lambda s^{\alpha+1})\bar{v}(r,s)$$
$$-\frac{P_0}{r}\left[\left(1+\lambda\omega^{\alpha}\cos\left(\frac{\pi}{2}\alpha\right)\right)\frac{\omega}{s^2+\omega^2}+\lambda\omega^{\alpha}\sin\left(\frac{\pi}{2}\alpha\right)\frac{s}{s^2+\omega^2}\right]$$
$$=\upsilon\left(1+\lambda_r s^{\delta}\right)\left(\frac{\partial^2}{\partial r^2}+\frac{1}{r}\frac{\partial}{\partial r}-\frac{1}{r^2}\right)\bar{v}(r,s) \quad (13)$$

The finite Hankel transform is as follows:

$$\mathcal{H}_n\{f(r)\}=\tilde{f}(k_\gamma)=\int_{R_1}^{R_2} rf(r)A_n(rk_\gamma)dr \qquad R_2>R_1 \qquad 14)$$

Where $A_n(rk_\gamma)=J_n(rk_\gamma)Y_n(R_1k_\gamma)-Y_n(rk_\gamma)J_n(R_1k_\gamma).\,k_\gamma$, stands for the positive roots of $A_n(rk_\gamma)=0$, where $J_n(.)$ and $Y_n(.)$, stand for the first order and second order n Bessel functions, separately. At this instant, multiply Equation (13) by $rA_n(rk_\gamma)$ and integrating from R_1 to R_2 concerning r using the identity:

$$\int_{R_1}^{R_2} r\left(\frac{\partial^2}{\partial r^2}+\frac{1}{r}\frac{\partial}{\partial r}-\frac{1}{r^2}\right)\bar{v}(r,s)\,A_1(rk_\gamma)dr=$$
$$-\frac{2}{\pi}\frac{f}{s-a}\frac{J_1(R_2k_\gamma)}{J_1(R_1k_\gamma)}-{k_\gamma}^2\bar{v}_H(k_\gamma,s) \quad (15)$$

Finally, we arrive at:

$$\bar{v}_H=P_0\left(1+\lambda\omega^{\alpha}\cos\left(\frac{\pi}{2}\alpha\right)\right)\frac{s}{(s^2+\omega^2)(s+\lambda s^{\alpha+1}+\upsilon k_\gamma^2)}$$
$$\times\frac{\overline{A_1}(R_1k_\gamma)-\overline{A_1}(R_2k_\gamma)}{k_\gamma}$$
$$-P_0\lambda\omega^{\alpha}\sin\left(\frac{\pi}{2}\alpha\right)\frac{\omega}{(s^2+\omega^2)(s+\lambda s^{\alpha+1}+\upsilon k_\gamma^2)}$$
$$\times\frac{\overline{A_1}(R_1k_\gamma)-\overline{A_1}(R_2k_\gamma)}{k_\gamma}-\frac{2}{\pi}\frac{f}{s-a}\frac{J_1(R_2k_\gamma)}{J_1(R_1k_\gamma)}$$
$$\times\frac{\upsilon\left(1+\lambda_r s^{\delta}\right)}{s+\lambda s^{\alpha+1}+\upsilon k_\gamma^2} \quad (16)$$

In which $\overline{A_1}(rk_\gamma)=J_0(rk_\gamma)Y_1(R_2k_\gamma)-J_1(R_2k_\gamma)Y_0(rk_\gamma)$. As described by (Fang & Liu., 2020) in Y_0 (rk_γ). The following is an appropriate way to write the Equation (16):

$$\bar{v}_H = P_0\left(1+\lambda\omega^{\alpha}\cos\left(\frac{\pi}{2}\alpha\right)\right)\frac{\omega}{(s^2+\omega^2)(s+\lambda s^{\alpha+1}+\upsilon k_\gamma^2)} \times \frac{\overline{A_1}(R_1k_\gamma)-\overline{A_1}(R_2k_\gamma)}{k_\gamma} - P_0\lambda\omega^{\alpha}\sin\left(\frac{\pi}{2}\alpha\right)\frac{s}{(s^2+\omega^2)(s+\lambda s^{\alpha+1}+\upsilon k_\gamma^2)} \times \frac{\overline{A_1}(R_1k_\gamma)-\overline{A_1}(R_2k_\gamma)}{k_\gamma} - \frac{2}{\pi k_\gamma^2}\frac{f}{s-a}\frac{J_1(R_2k_\gamma)}{J_1(R_1k_\gamma)} - \frac{2f}{\pi k_\gamma^2}\frac{J_1(R_2k_\gamma)}{J_1(R_1k_\gamma)}\frac{\lambda_r s^{\delta}-(s+\lambda s^{\alpha+1})}{(s-a)(s+\lambda s^{\alpha+1}+\upsilon k_\gamma^2)} \quad (17)$$

The inverse Hankel transform is as follows:

$$\bar{v}(r,s) = \frac{\pi^2}{2}\sum_{\gamma=1}^{\infty}\frac{{k_\gamma}^2{J_1}^2(R_1k_\gamma)A_1(rk_\gamma)}{{J_1}^2(R_1k_\gamma)-{J_1}^2(R_2k_\gamma)}\bar{v}_H(k_\gamma,s) \quad (18)$$

Applying Inverse Hankel transform on Equation (17) using Equation (18) and the well-known result, we find that,

$$\frac{s}{(s^2+\omega^2)(s+\lambda s^{\alpha+1}+\upsilon k_\gamma^2)} = -\frac{s}{(s^2+\omega^2)}\frac{1}{\lambda}\sum_{i=0}^{\infty}\left(-\frac{1}{\lambda}\right)^{i+1}\frac{s^i}{\left(s^{\alpha+1}+\upsilon k_\gamma^2\lambda^{-1}\right)^{i+1}} \quad 19)$$

The equation obtained is:

$$\bar{v}(r,s) = \frac{R_1\left({R_2}^2-r^2\right)}{\left({R_2}^2-{R_1}^2\right)r}\frac{f}{s-a} + \frac{\pi^2P_0}{2}\left(1+\lambda\omega^{\alpha}\cos\left(\frac{\pi}{2}\alpha\right)\right)\times \sum_{\gamma=1}^{\infty}\frac{k_\gamma{J_1}^2(R_1k_\gamma)A_1(rk_\gamma)\left[\overline{A_1}(R_1k_\gamma)-\overline{A_1}(R_2k_\gamma)\right]}{{J_1}^2(R_1k_\gamma)-{J_1}^2(R_2k_\gamma)}\frac{\omega}{(s^2+\omega^2)(s+\lambda s^{\alpha+1}+k_\gamma^2)} + \frac{\pi^2P_0}{2}\lambda\omega^{\alpha}\sin\left(\frac{\pi}{2}\alpha\right)\sum_{\gamma=1}^{\infty}\frac{k_\gamma{J_1}^2(R_1k_\gamma)A_1(rk_\gamma)\left[\overline{A_1}(R_1k_\gamma)-\overline{A_1}(R_2k_\gamma)\right]}{{J_1}^2(R_1k_\gamma)-{J_1}^2(R_2k_\gamma)}\times -\pi f\sum_{\gamma=1}^{\infty}\frac{J_1(R_1k_\gamma)J_1(R_2k_\gamma)A_1(rk_\gamma)}{{J_1}^2(R_1k_\gamma)-{J_1}^2(R_2k_\gamma)}\frac{\lambda_r s^{\delta}}{(s-a)(s+\lambda s^{\alpha+1}+k_\gamma^2)} + \pi f\sum_{\gamma=1}^{\infty}\frac{J_1(R_1k_\gamma)J_1(R_2k_\gamma)A_1(rk_\gamma)}{{J_1}^2(R_1k_\gamma)-{J_1}^2(R_2k_\gamma)}\frac{(s+\lambda s^{\alpha+1})}{(s-a)(s+\lambda s^{\alpha+1}+k_\gamma^2)} \quad (20)$$

In the end, using the convolution theorem and the function $G_{l,m,n}(c,t)$ (Lorenzo & Carl, 2008), when the discrete inverse Laplace transform is applied to (20) the velocity field is demonstrated as follows:

$$v = \frac{R_1\left({R_2}^2-r^2\right)f}{\left({R_2}^2-{R_1}^2\right)r}e^{at} -$$

$$\frac{\pi^2 P_0}{2}\left(1+\lambda\omega^{\alpha}\cos\left(\frac{\pi}{2}\alpha\right)\right)\sum_{\gamma=1}^{\infty}\frac{k_\gamma {J_1}^2(R_1k_\gamma)A_1(rk_\gamma)\left[\overline{A_1}(R_1k_\gamma)-\overline{A_1}(R_2k_\gamma)\right]}{{J_1}^2(R_1k_\gamma)-{J_1}^2(R_2k_\gamma)}\times$$
$$\sum_{i=0}^{\infty}\left(-\frac{1}{\lambda}\right)^{i+1}\int_0^t \sin[\beta\ \ (t-\tau)]\left[G_{\alpha+1,i,i+1}\left(-\upsilon {k_\gamma}^2\lambda^{-1},\tau\right)\right]d\tau -$$
$$\frac{\pi^2 P_0}{2}\lambda\omega^{\alpha}\sin\left(\frac{\pi}{2}\alpha\right)\sum_{\gamma=1}^{\infty}\frac{k_\gamma {J_1}^2(R_1k_\gamma)A_1(rk_\gamma)\left[\overline{A_1}(R_1k_\gamma)-\overline{A_1}(R_2k_\gamma)\right]}{{J_1}^2(R_1k_\gamma)-{J_1}^2(R_2k_\gamma)}\times$$
$$\sum_{i=0}^{\infty}\left(-\frac{1}{\lambda}\right)^{i+1}\int_0^t \cos[\beta\ \ (t-\tau)]\left[G_{\alpha+1,i,i+1}\left(-\upsilon {k_\gamma}^2\lambda^{-1},\tau\right)\right]d\tau +$$
$$\pi f\sum_{\gamma=1}^{\infty}\frac{J_1(R_1k_\gamma)J_1(R_2k_\gamma)A_1(rk_\gamma)}{{J_1}^2(R_1k_\gamma)-{J_1}^2(R_2k_\gamma)}\sum_{i=0}^{\infty}\left(-\frac{1}{\lambda}\right)^{i+1}\lambda_r\int_0^t e^{a(t-\tau)}\left[G_{\alpha+1,i+\delta,i+1}\left(-\upsilon {k_\gamma}^2\lambda^{-1},\tau\right)\right]d\tau -$$
$$\pi f\sum_{\gamma=1}^{\infty}\frac{J_1(R_1k_\gamma)J_1(R_2k_\gamma)A_1(rk_\gamma)}{{J_1}^2(R_1k_\gamma)-{J_1}^2(R_2k_\gamma)}\sum_{i=0}^{\infty}\left(-\frac{\upsilon {k_\gamma}^2}{\lambda}\right)^{i+1}\int_0^t e^{a(t-\tau)}\left[G_{\alpha,-i,i}(-\lambda^{-1},\tau)\right]d\tau \quad 21)$$

Where $G_{l,m,n}(c,t)=\sum_{j=0}^{\infty}\frac{(n)_j c^j t^{-(n+j)m-l+1}}{j!\Gamma(n+j)^{l-m}}$ is the generalized G function. $(n)_j$ represents the Pochhammer polynomial, and the velocity manifestation given in Equation (21) remains the same as the solutions proposed in Liancun et al. (2011), if the outer cylinder is assumed to be fixed however the inner cylinder is moving.

Computation of the Shear Stress

Using the Laplace transform on Equation (7), one can obtain,

$$\bar{\tau}(r,s)=\frac{\mu\left(1+\lambda_r s^{\delta}\right)}{(1+\lambda s^{\alpha})}\left(\frac{\partial}{\partial r}-\frac{1}{r}\right)\bar{v}(r,s) \qquad (22)$$

Equation (22), which uses Equation (21) achieved:

$$\bar{\tau}(r,s)=\frac{\mu\left(1+\lambda_r s^{\delta}\right)}{(1+\lambda s^{\alpha})}\frac{2R_1R_2}{\left({R_2}^2-{R_1}^2\right)r^2}\left(\frac{R_1\omega_2\beta_2}{s^2+{\beta_2}^2}-\frac{R_2\omega_1\beta_1}{s^2+{\beta_1}^2}\right)+$$
$$\mu\pi\sum_{\gamma=1}^{\infty}\frac{{J_1}^2(R_1k_\gamma)\left[\frac{2}{r}A_1(rk_\gamma)-k_\gamma\overline{A_1}(rk_\gamma)\right]}{{J_1}^2(R_1k_\gamma)-{J_1}^2(R_2k_\gamma)}\left[\frac{\omega_2\beta_2}{s^2+{\beta_2}^2}-\right.$$
$$\left.\left[\frac{\omega_1\beta_1}{s^2+{\beta_1}^2}\frac{J_1(R_2k_\gamma)}{J_1(R_1k_\gamma)}\right]\frac{s\left(1+\lambda_r s^{\delta}\right)}{\upsilon {k_\gamma}^2+\upsilon {k_\gamma}^2\lambda_r s^{\delta}+s+\lambda s^{\alpha+1}}+\right.$$
$$\frac{\mu\pi}{2}\sum_{\gamma=1}^{\infty}\frac{k_\gamma {J_1}^2(R_1k_\gamma)\left[\frac{2}{r}A_1(rk_\gamma)-k_\gamma\overline{A_1}(rk_\gamma)\right]}{{J_1}^2(R_1k_\gamma)-{J_1}^2(R_2k_\gamma)}\frac{\rho P_0\omega\left[\overline{A_1}(R_1k_\gamma)-\overline{A_1}(R_2k_\gamma)\right]}{(s^2+\omega^2)}\times$$
$$\frac{\left(1+\lambda_r s^{\delta}\right)}{\upsilon {k_\gamma}^2+\upsilon {k_\gamma}^2\lambda_r s^{\delta}+s+\lambda s^{\alpha+1}} \qquad (23)$$

Like this, the equation described below is obtained with the help of the generalized R function.

$$\tau(r,t)=\frac{2\mu R_1R_2}{\lambda\left({R_2}^2-{R_1}^2\right)r^2}\int_0^t[R_1\omega_2 sin\,\beta_2(t-\tau)-$$
$$R_2\omega_1\,sin\,\beta_1(t-\tau)]\left[R_{\alpha,0}(-\lambda^{-1},t)+\lambda_r R_{\alpha,\delta}(-\lambda^{-1},t)\right]d\tau+$$
$$\frac{\mu\pi}{\lambda}\sum_{\gamma=1}^{\infty}\frac{{J_1}^2\left(R_1k_\gamma\right)[\frac{2}{r}A_1\left(rk_\gamma\right)-k_\gamma\overline{A_1}\left(rk_\gamma\right)]}{{J_1}^2\left(R_1k_\gamma\right)-{J_1}^2\left(R_2k_\gamma\right)}\times$$
$$\sum_{i=0}^{\infty}\sum_{q=0}^{i}\frac{i!}{q!\,(i-q)!}\left(\frac{\upsilon{k_\gamma}^2}{\lambda}\right)^i\times{\lambda_r}^q\int_0^t[\omega_2\,sin\,\beta_2\,(t-\tau)-$$
$$\omega_1 sin\,\beta_1\,(t-\tau)\frac{J_1\left(R_2k_\gamma\right)}{J_1\left(R_1k_\gamma\right)}]\left[G_{\alpha,\delta q-i,1+i}(\tau,-\lambda^{-1})+\quad\lambda_r G_{\alpha,\delta q+\delta-i,1+i}(\tau,-\lambda^{-1})\right]d\tau$$
$$-\frac{\mu\pi}{2\lambda}\sum_{\gamma=1}^{\infty}\frac{{J_1}^2\left(R_1k_\gamma\right)\left[\frac{2}{r}A_1\left(rk_\gamma\right)-k_\gamma\overline{A_1}\left(rk_\gamma\right)\right]}{{J_1}^2\left(R_1k_\gamma\right)-{J_1}^2\left(R_2k_\gamma\right)}\times$$
$$\sum_{i=0}^{\infty}(\sum_{q=0}^{i}\frac{i!}{q!\,(i-q)!}\left(\frac{\upsilon{k_\gamma}^2}{\lambda}\right)^i)\times{\lambda_r}^q k_\gamma P_0\left[\overline{A_1}\left(R_1k_\gamma\right)-\overline{A_1}\left(R_2k_\gamma\right)\right]$$
$$\int_0^t sin\,\omega(t-\tau)\left[G_{\alpha,\delta q-i-1,i+1}(\tau,-\lambda^{-1})\right.$$
$$\left.+\;\lambda_r G_{\alpha,\delta q+\delta-i-1,i+1}(\tau,-\lambda^{-1})\right]d\tau \qquad (24)$$

$Where\quad R_{l,m}(d,t)=\sum_{j=0}^{\infty}\frac{d^j t^{(j+1)m-l-1}}{\Gamma[(j+1)l-m]}$.

The shear stress Equation (24) agrees with the findings (Liancun et al., 2011).

Analysis of Results and Discussion

Using the Caputo fractional operator and integral transform, this paper examined the velocity profile and shear stress for the fractionalized Oldroyd-B fluid flow in a rotating cylinder utilizing an oscillating pressure gradient. By applying finite Hankel and Laplace transforms to the successive fractional derivatives, the velocity field and the appropriate shear stress are found. The results are given in the provision of the generalized G and Mittag-Leffler functions using integral and series forms. For the different cases, while $\alpha \rightarrow 1$ for the Oldroyd B fluid *and* $\alpha \rightarrow 1$ *and* $\lambda_r \rightarrow 0$, we acquire the equivalent solution of a classical Newtonian fluid. In Equations (21) and (24) respectively, the effects of influential factors on the fluid's velocity and shear stress are defined. SI units are utilised for all numbers and the roots are predictable by $k_\gamma =$

$\frac{(2r-1)\pi}{R_2-R_1}$. Graphical representations of the velocity field v(r,t) and shear stress (r,t) were created alongside r for a range of t values and important factors to show how the findings physically manifested. For the computation and graphical results, Mathematica 7 is utilized.

The time effect on the fluid velocity is epitomized in Figure 2, in contrast to regular Oldroyd B fluid and fractionalized Oldroyd B fluid, when r gets near R_1, the velocity declines as a function of t. In addition, Fractionalized Oldroyd B fluid exhibits a larger fluctuation amplitude. As we can see in Figure 3, at larger values of α, there is a decrease in velocity and a smaller fluctuation.

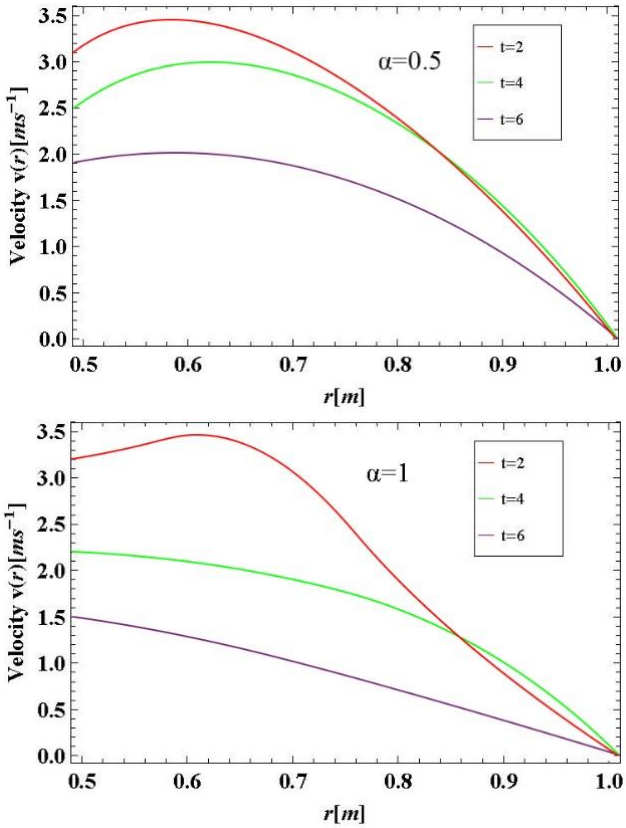

Figure 2: Velocity profiles for different values of time $(\boldsymbol{R_1 = 0.5, R_2 = 1,\ \omega = 0.1,\ \lambda = 10,\ \lambda_r = 2,\ \upsilon = 0.2, a = -0.2, f = 4, P_0 = 2})$.

A visual representation of the relaxation parameter λ is shown in Figure 4. It demonstrates that as the magnitude of λ increases the variations between two circular cylinders get larger and larger. This may be caused by viscous forces becoming less potent as λ values rise, in

contrast to Figure 5, which shows the reverse pattern for the retardation parameter λ_r. Figure 6 illustrates the association between kinematic viscosity and velocity, showing that as fluid kinematic viscosity increases, decreases velocity. Because an increase in viscosity provides resistance to fluid flow, which lowers the fluid's velocity, this relationship physically confirms our findings. The limiting cases for the material constant λ_r for the conventional Oldroyd-B fluid ($\alpha \rightarrow 1$ or $\alpha \rightarrow 1$ and $\lambda_r \rightarrow 0$) are depicted in Figure 7. For the various values of the radial distance r, the time series of the velocity profiles are displayed in Figure 8. We can see that the velocity increases and drops simultaneously, reaching its maximum in the radius range of 0.65–0.75. The fluctuating velocity in this profile is caused by the oscillating pressure gradient. The fluctuations increase from 0.6 to 0.7 and reach 0.95; nevertheless, the velocity profiles fluctuate less for both the ordinary and fractionalized Oldroyd-B fluids. As α decreases from 1 to 0, the oscillation period is longer.

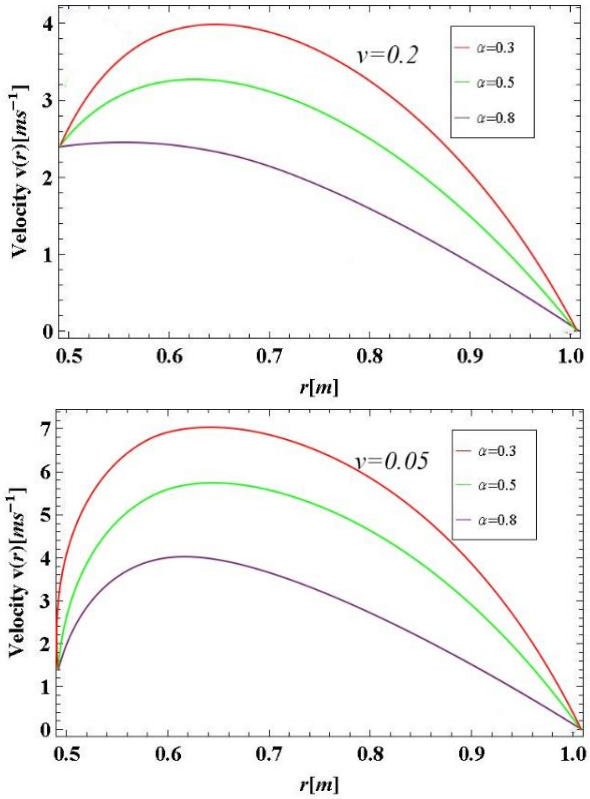

Figure 3: Velocity profile for different values of the fractional parameter α $(R_1 = 0.5,\ R_2 = 1, t = 4, \omega = 0.1, \lambda = 10, \lambda_r = 2, a = -0.2, f = 4, P_0 = 2.$

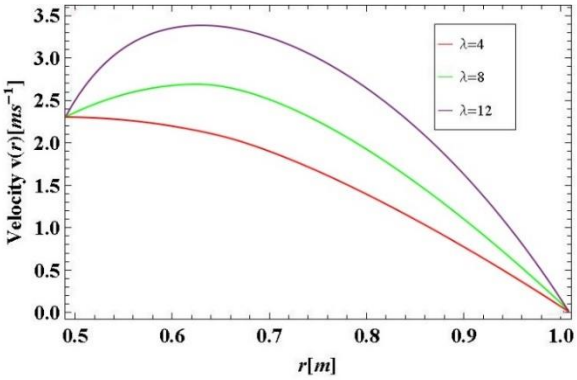

Figure 4: Velocity profile for different values of λ ($\alpha = 0.5, t = 4, R_1 = 0.5, R_2 = 1, \omega = 0.1, \lambda_r = 2, \upsilon = 0.2, a = -0.2, f = 4, P_0 = 2$).

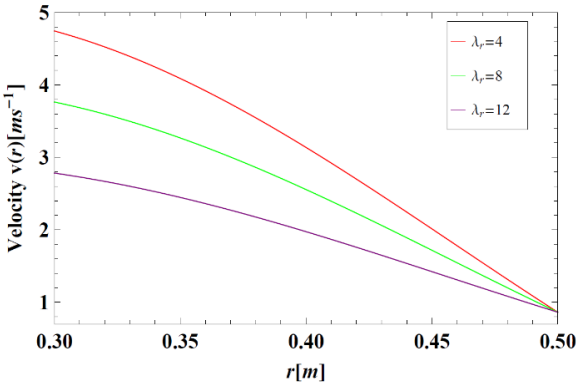

Figure 5: Velocity profile for different values of λ_r ($\alpha = 0.5, t = 4, R_1 = 0.5, R_2 = 1, \omega = 0.1, \lambda = 2, \upsilon = 0.2, a = -0.2, f = 4, P_0 = 2$).

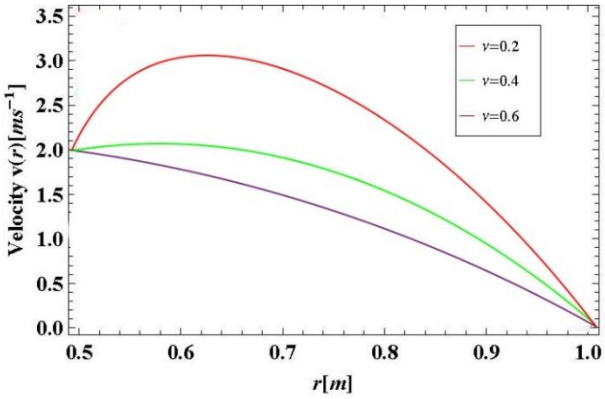

Figure 6: Velocity profile for different values of kinematic viscosity ($\lambda = 120, \alpha = 0.5, t = 4, R_1 = 0.5, R_2 = 1, \omega = 0.1, \lambda_r = 2, a = -0.2, f = 4, P_0 = 2$).

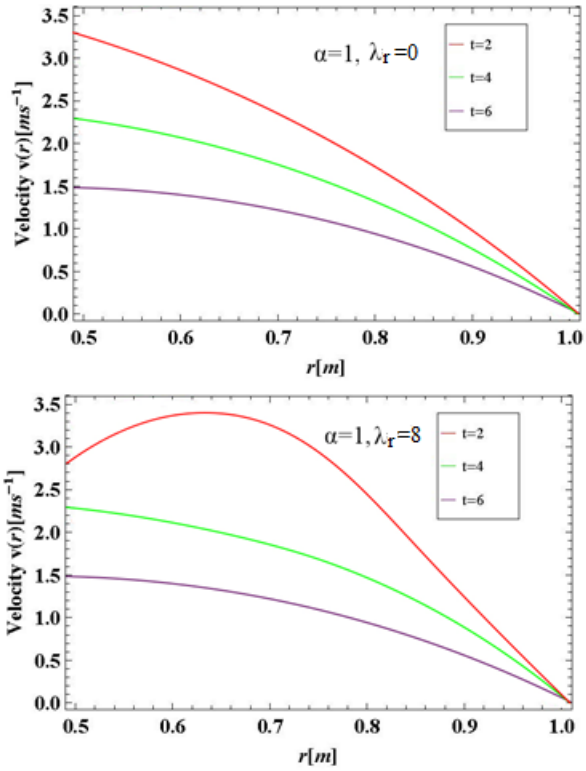

Figure 7: Velocity profile for different values of t ($R_1 = 0.5, R_2 = 1, \omega = 0.1, \lambda = 2, \upsilon = 0.2, a = -0.2, P_0 = 2$).

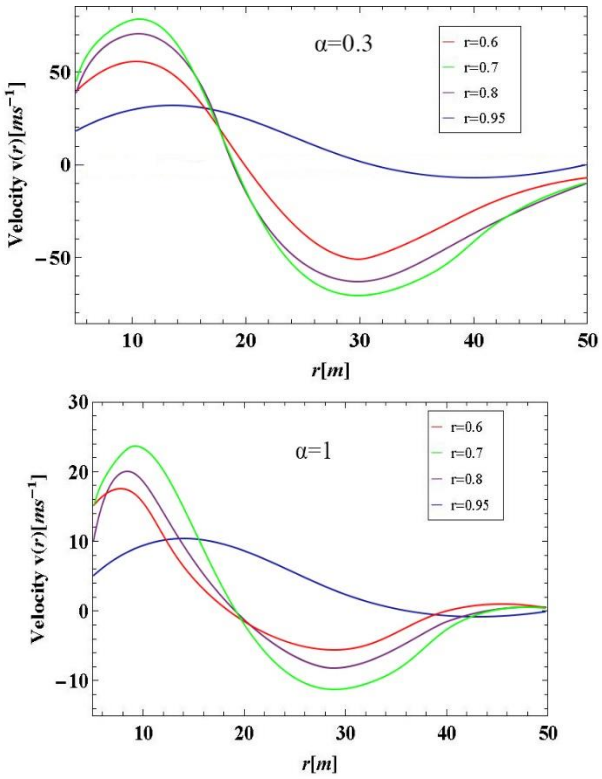

Figure 8: Velocity profile for different values of $(\lambda = 15, R_1 = 0.5, R_2 = 1, \omega = 0.1, \lambda_r = 2, \upsilon = 0.03, a = -0.2, f = 15, P_0 = 10$.

Conclusion

The goal of this work is to study the Oldroyd-B fluid flow between coaxial cylinders that are moving as a result of a pressure gradient that varies over time. The classical model is then generalized using the Caputo fractional derivative, which has recently become the most widely used fractional derivative. Analytical solutions are then obtained by applying the Laplace and Hankel transform techniques. The graphs also display the gathered results. The main results obtained are given as follows. Variability in every profile are displayed for various values of α. This result illustrates the fluid's memory effect, which the integer order derivative is unable to convey. Velocity for the fractionalized Oldroyd-B fluid declines with increasing time. The amount of kinematic viscosity is inversely related to the rate of velocity. Both non-Newtonian parameters, λ and λ_r, have opposite effects on the motion of the fluid. With increasing relaxation parameter, dominant oscillations are seen. The current findings

can possibly be simplified to the classical Oldroyd-B, Maxwell fluid, and classical Newtonian fluid models by assuming that $\alpha \rightarrow 1$, $\lambda_r \rightarrow 0$.

Nomenclature	
P	The Hydrostatic density(kgm^{-3})
v	Velocity (ms^{-1})
S	Extra stress tensor(Nm^{-2})
τ	Shear stress(Nm^{-2})
P	The pressure (Pa)
R_1	The radius of the inner cylinder(m)
R_2	The radius of the outer cylinder(m)
μ	Dynamic viscosity($kgm^{-2}s^{-2}$)
υ	Kinematic viscosity(m^2s^{-1})
α, δ	Fractional parameters (s)
λ	Relaxation parameter (s)
λ_r	Retardation parameter (s)
β_2	Angular velocity of the inner cylinder($rad\ s^{-1}$)
β_2	Angular velocity of the outer cylinder($rad\ s^{-1}$)

References

Miller, K. S., & Ross, B. (1993). An introduction to the fractional calculus and fractional differential equations.

Rauf, A., Rubbab, Q., Vieru, D., & Majeed, A. (2020). Simultaneous flow of two immiscible fractional maxwell fluids with the clear region and homogeneous porous medium. *Sains Malaysiana*, *49*(11), 2871-2880.

Khalique, C. M., Safdar, R., & Tahir, M. (2019). First analytic solution for the oscillatory flow of a Maxwell's fluid with annulus. *Open Journal of Mathematical Sciences*, *3*(1), 159-166.

Shaikh, K., Shaikh, F., Khokhar, R. B., & Memon, K. N. (2022). Analytical Solution of Transient Flow of Fractional Oldroyd-B Fluid between Oscillating Cylinders. *VFAST Transactions on Mathematics*, *10*(2), 21-33.

Qureshi, S., Yusuf, A., Shaikh, A. A., Inc, M., & Baleanu, D. (2019). Fractional modeling of blood ethanol concentration system with real data application. *Chaos: An Interdisciplinary Journal of Nonlinear Science*, *29*(1).

Qureshi, S., & Jan, R. (2021). Modeling of measles epidemic with optimized fractional order under Caputo differential operator. *Chaos, Solitons & Fractals*, *145*, 110766.

Khaskheli, M. A., Memon, K. N., Sheikh, A. H., Siddiqui, A. M., & Shah, S. F. (2020). Tank drainage for an electrically conducting

newtonian fluid with the use of the bessel function. *Eng. Technol. Appl. Sci. Res*, *10*(2), 5377-5381.

Tanveer, M., Ullah, S., Khan, N. A., Khan, N. A., & Rehman, N. (2017). MHD flow of generalized Oldroyd-B fluid over an infinite oscillating plate with slip condition using Fox H-function. *Journal of Computational and Theoretical Nanoscience*, *14*(3), 1362-1370.

Bhutto, A. A., Shah, S. F., Khokhar, R. B., Harijan, K., & Hussain, M. (2023). To Investigate Obstacle Configuration Effect on Vortex Driven Combustion Instability. *VFAST Transactions on Mathematics*, *11*(1), 67-82.

Qureshi, S., & Yusuf, A. (2019). Mathematical modeling for the impacts of deforestation on wildlife species using Caputo differential operator. *Chaos, Solitons & Fractals*, *126*, 32-40.

Bhutto, A. A., Ahmed, I., Rajput, S. A., & Shah, S. A. R. (2023). The effect of oscillating streams on heat transfer in viscous magnetohydrodynamic MHD fluid flow. *VFAST Transactions on Mathematics*, *11*(1), 1-16.

Khokhar, R. B., Bhutto, A. A., Bhutto, I. A., Shaikh, F., Memon, K. N., & Kumar, P. (2024). A numerical analysis of mixing and separating of newtonian fluids in a channel filled with porous materials. *Mehran University Research Journal Of Engineering & Technology*, *43*(2), 46-64.

Oldroyd, J. G. (1950). On the formulation of rheological equations of state. *Proceedings of the Royal Society of London. Series A. Mathematical and Physical Sciences*, *200*(1063), 523-541.

Debnath, L., & Bhatta, D. (2016). *Integral transforms and their applications*. Chapman and Hall/CRC.

Lorenzo, C. F., & Hartley, T. T. (1999). Generalized functions for the fractional calculus.

Zheng, L., Li, C., Zhang, X., & Gao, Y. (2011). Exact solutions for the unsteady rotating flows of a generalized Maxwell fluid with oscillating pressure gradient between coaxial cylinders. *Computers & Mathematics with Applications*, *62*(3), 1105-1115.